Theoretical Chemistry Accounts (2023) 142:81
https://doi.org/10.1007/s00214-023-03013-9

RESEARCH

Influence of Lewis acids on the symmetric S_N2 reaction

Iñigo Iribarren[1] · Cristina Trujillo[1,2] · Goar Sánchez-Sanz[3,4] · Eric Hénon[5] · José Elguero[6] · Ibon Alkorta[6]

Received: 14 April 2023 / Accepted: 13 July 2023 / Published online: 5 August 2023

Abstract
This paper presents a theoretical analysis the effect of non-covalent interactions (NCI) in three different S_N2 reactions ($X^-:CH_3X \rightarrow XCH_3:X^-$, X = Cl, Br and I) has been theoretically analysed in the pre-reactive complexes, TS and products. A total of eighteen Lewis acids (LAs: FH, ClH, FCl, I_2, SeHF, SeF_2, PH_2F, PF_3, SiH_3F, SiF_4, BH_3, BF_3, BeH_2, BeF_2, LiH, LiF, Au_2 and AgCl) interact with the halogen atom of the CH_3X molecule. To analyse the strength of the non-covalent interactions, both the independent gradient model tool and electron density maps have been employed. The results reveal that in all cases, the interaction between the anion and the Lewis acid leads to an increase in the transition barriers compared to the parental reaction.

Keywords S_N2 · Lewis acid · Non-covalent interactions · Electron density shifts · Independent gradient model

1 Introduction

Introduced by Hughes and Ingold in 1935 [1–3] the binuclear nucleophilic substitution, S_N2 reaction is one of the principal backbones in organic chemistry [4], corresponding to a mechanism where one bond is broken and one bond is formed synchronously. The S_N2 reaction is closely linked to the Walden inversion [5–7] and to the Finkelstein reaction (an S_N2 reaction that involves the exchange of one halogen for another) [8]. The S_N2 reaction has been much studied over the years [9], especially from a theoretical perspective by Bickelhaupt et al. [10–15]. These authors have extensively examined the reaction, particularly focusing on solvent effects [13, 14]. Garver et al. observed that the S_N2 reaction between CN^- and CH_3I proceeds through a double-well energy pathway in gas phase, while the inclusion of solvent effects, transforms the reaction in a unimodal pathway [16]. While the influence of solvent effects has garnered significant attention in the literature with numerous dedicated papers [17–21], the importance of the gas-phase studies cannot be overlooked.These studies offer valuable and intricate insights into the underlying reaction mechanisms. Gas-phase studies contribute to a more comprehensive comprehension of the process [19, 22–26].

Bierbaum et al. have studied the effect of microsolvated anions on S_N2 reactions and compared those with gas phase result [16, 24, 25]. In order to model the microsolvated anions, the authors used an explicit solvent molecule interacting with the respective anion and found an enhanced reactivity within solvated anions. Furthermore, in a separate investigation, it was studied how α-nucleophiles (R-Y-X^-) enhance the reactivity in S_N2 reaction with respect to the normal nucleophiles (R-X^-) reducing dramatically the transition barriers [27].

The study of the S_N2 reaction has not only been limited to carbon-centred reactions but also expanded into N, O, F, Si, P centres [26, 28–32] and also for both cationic and anionic systems [33–36]. It is worth mentioning that in addition to

✉ Goar Sánchez-Sanz
goar.sanchezsanz@manchester.ac.uk

✉ Ibon Alkorta
ibon@iqm.csic.es

1 Trinity Biomedical Sciences Institute, School of Chemistry, Trinity College, The University of Dublin, Dublin 2, Ireland

2 Department of Chemistry, The University of Manchester, Oxford Road, Manchester M13 9PL, UK

3 Irish Centre of High-End Computing, Grand Canal Quay, Dublin 2, Ireland

4 Kilburn Building, The University of Manchester, Oxford Road, Manchester M13 9PL, UK

5 Institut de Chimie Moléculaire de Reims, UMR CNRS 7312, Université de Reims Champagne-Ardenne, BP39, 51687 Reims CEDEX 02, France

6 Instituto de Química Médica (CSIC), Juan de La Cierva, 3, 28006 Madrid, Spain

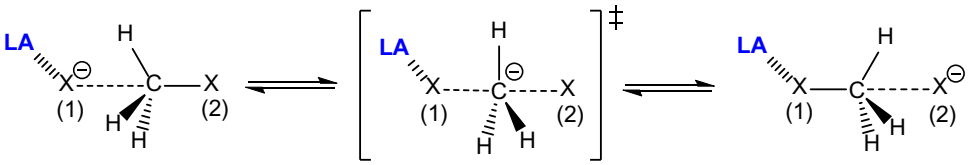

Scheme 1 S_N2 reactions studied. X = Cl, Br and I in the present study. The numbering used along the article for the two different X atoms is indicated

the most common experimental and theoretical methodologies, other authors have explored the S_N2 reaction by means of the interacting quantum atom methodology [37, 38] and the kinetic isotopic effects [39]. Uggerud et al. studied the steric and electronic effects on S_N2 reactions and by using electron density shift (EDS) results, provided an alternative interpretation of the factors that govern the reaction [40, 41]. It is clear that there is a plethora of articles devoted to the S_N2 reaction with numerous recent reviews available [13, 19, 41].

The catalysis using Lewis acids (LAs) have been experimentally explored in S_N2-type ring openings [42–44] and from the theoretical point of view in other reactions, *i.e.* Diels–Alder [45, 46]. Those LAs interact with the anions through so-called non-covalent interactions (NCI) [47]. Given the importance of the subject, and very intrigued by the effect of a third-party molecule within the S_N2 reaction, we decided to study how LAs influence the mentioned reaction.

Herein, to analyse the effect of the LA on the potential energy profiles, the selection of symmetric S_N2 reactions allows for the straightforward acquisition and analysis of transition barriers.

In the present article, the effect of a large variety of NCIs [47] (hydrogen [48, 49], halogen [50–52], chalcogen [53–55], pnictogen [56–58], tetrel [59–61], triel [62, 63], beryllium [64, 65], lithium [66, 67] and regium bonds [68–70]) in three S_N2 reactions has been studied where a LA interacts with one of the halogen atoms involved in the reaction. For each system, three stationary points have been characterised along the reaction coordinate: (1) two minima: pre-reaction assembly complex (Scheme 1, l.h.s.) and product complex (Scheme 1, r.h.s.) and (2) the transition state (TS) (at the centre of Scheme 1) linking them. The influence of the NCIs on the geometry, energy and electronic properties of these systems has been analysed.

2 Computational details

2.1 Ab initio calculations

The systems under study have been optimised using the M06-2X DFT computational method [71] and the 6–311++G(d,p) basis set [72]. The effective core potential def2-TZVPD basis set [73] has been used for the iodine, gold and silver. These methods have been proved to produce reliable results in S_N2 reactions [37] and in LAs within NCIs [74], compared with CCSD and CCSD(T) methodologies [75, 76]. Frequency calculations have been performed to verify that the geometries obtained correspond to energetic minima or true transition states (zero and one imaginary frequencies, respectively) and to obtain the thermodynamic parameters. These calculations have been carried out with the Gaussian-16 program [77]. All the Cartesian coordinates for all the complexes studies can be found in the Electronic Supporting Information.

Binding energies (ΔE_b) were calculated as the difference of the electronic energy of the optimised complex minus the electronic energy of each monomer in their optimised geometry. All the binding energies have been corrected with the basis set superposition error (BSSE) [78].

Independent gradient model–intrinsic bond strength index (*IGM–IBSI)* method: IGM is a recent electron density (ED) overlap-based computational method that enables to detect and quantify covalent and non-covalent chemical interactions [79, 80]. It employs a descriptor, δg, which locally quantifies the electron density clash between two given sources (atoms or fragments or molecules). In other words, δg accounts for the tendency of electrons to be shared between defined fragments. In this study, the ED was calculated from the wave function obtained after the DFT optimisation geometry.

The 2D plot of δg (collected for every node of a three-dimensional grid enclosing the system) as a function of the signed ED leads to a picture where one or more peaks (δg^{peak}) appear, leading to a specific signature of the interaction; the larger the peak, the more intense the interaction. In the IGM framework, weak NCI hardly exceed a δg^{peak} of 0.1 a.u. Hydrogen bond generally may extend up to a maximum of $\delta g^{peak} = 0.1$ a.u. ($\delta g^{peak} = 0.06$ a.u. for HB in water dimer), while vdW interactions rarely extend beyond 0.02–0.03 a.u. Pure covalent bonds range from 0.2 up to around 2.5 a.u. Metal coordination δg^{peak} values range between 0.1 and 0.6 a.u.

Moreover, in this study, the following integration scheme has been used to quantify the interaction between the LA and the S_N2 system:

$$\Delta g = \int_v \delta g \mathrm{d}v \quad (1)$$

(dv is an elementary volume related to the grid enclosing the chemical system).

Furthermore, the IGM–IBSI integrated index [81] has been employed to probe the effect of the LA on the strength of the X–C covalent bond to be broken during the reaction. For an in-depth understanding of various IGM aspects, the reader may refer to the original work [79, 80]. All calculations have been carried out using IGMPlot program [82].

2.2 Electron density shift

The electron density shift maps and the corresponding values were obtained as:

$$EDS_{XY} = \rho_{XY} - \left(\rho_X + \rho_Y\right) \quad (2)$$

where $\rho_{XY,}$ ρ_X and ρ_Y correspond to the electron density of the complex and both fragments, respectively. $EDS^+{}_T$ (total electron density shift) and $EDS+_{0.001}$ (electron density shift at the 0.001 au. isosurface) are calculated using a numerical grid from the density cubes using the following formula:

$$\sum_{i=1}^{N} \rho_+^{EDS}(i) = EDS_T^+ \quad (3)$$

where $\rho^{EDS}{}_+$ corresponds to the positive values of the electron density shift on each point of the grid upon complexation, so the sum of all those values corresponds to $EDS^+{}_T$. For the $EDS+_{0.001}$ term, only those points which fulfil the condition that the density value is equal or less than 0.001 a.u. are considered. The full procedure is described in ref. [83] and the code available in https://github.com/iribirii/EDS_quantification.

Figures were plotted using python and matplotlib [84], CYLview software [84] and VMD [85].

3 Results and discussion

This section has been organised as follows. First, the interaction between the LA and X^- with CH_3X constituents of the S_N2 reaction has been studied. Then, the effects of the LA on the S_N2 profile have been analysed and discussed with an emphasis on the geometrical and electronic effects on the reactants, transition states and final products. In each section, the intrinsic bond strength index (IBSI) and EDS analysis of the systems have been considered.

3.1 LA:X^- and LA:CH_3X complexes

The binding energies of each LA interacting with the isolated X^- and with CH_3X are shown in Fig. 1 and reported in Table S1. Binding energies for the LA···X^- are considerably more negative (between –57 and –262 kJ·mol^{-1}) than the ones found for LA···XCH_3 complexes (between −13 and −82 kJ·mol^{-1}). As expected, weak electron acceptors like HF or HCl show the smallest binding energies while strong Lewis acids, like LiH or AgCl present the largest (more negative) E_b values. It is also worth indicating that in LA···XCH_3 complexes, the differences between the halogen species are very small, except for Au_2 and AgCl in which the E_b for the three halogen derivatives (X = Cl, Br and I) are clearly differentiated. Furthermore, the binding energy values corresponding to X^-···H_3CX interaction in the binary complex are –49.0, –46.0 and –40.5 kJ·mol^{-1} (for X = Cl, Br and I, respectively). With all this above, it is clear that when the LA approaches the binary complex, it is expected that it will interact preferentially with the anion, X^-. Additionally, the binding energies between the LA and $[XCH_3X]^-$ moiety, interacting either on the anion side (LA···$[X···CH_3X]^-$) or on the XCH_3 side (LA···$[XCH_3···X]^-$, have been also analysed exhibiting the preferred binding mode mentioned above (Fig. 1).

Same behaviour has been found in the electron density shift (EDS) maps (Fig. 2), in which the interaction between the LA and the X^- displaces more electron density ($EDS^+{}_T$) that in the interaction with the XCH_3 moiety. This also occurs on the 0.001 a.u. electron density isosurfaces as indicated by the $EDS^+{}_{0.001}/EDS^-{}_{0.001}$ values.

This binding mode has been also corroborated by the IGM fingerprint, in which the calculated values of the δg^{peak} corresponding to the LA···X^- interactions complexes are larger than those of the analogous LA···XCH_3 ones for the same LA and X groups (Table S2).

Although the LA···X^- binding mode is preferred, it is worth shedding some information about the interaction of the LA with the XCH_3 for future works. In that regard, it is observed that LA with the XCH_3 interaction produces an elongation of the X–C bond as indication of the electron donation from the XCH_3 and weakening of this bond. The IGM–IBSI values of the X–C bonds recover this weakening showing smaller values as the X–C is longer. Also, linear relationships between the bond distance and the IBSI value for each halogen (Fig. S1) are obtained with $R^2 > 0.97$. As demonstrated later in this paper, the linear relationships are due to the small range of interatomic distances considered here, and when a wider range of distances are considered, exponential relationship is found.

3.2 Effect of LA on the S_N2 profile

3.2.1 Energetics

It has been stated unequivocally that the LA···X^- binding mode is preferred over the LA···XCH_3 complexation mode. In the following subsection, we monitor the fate of this LA

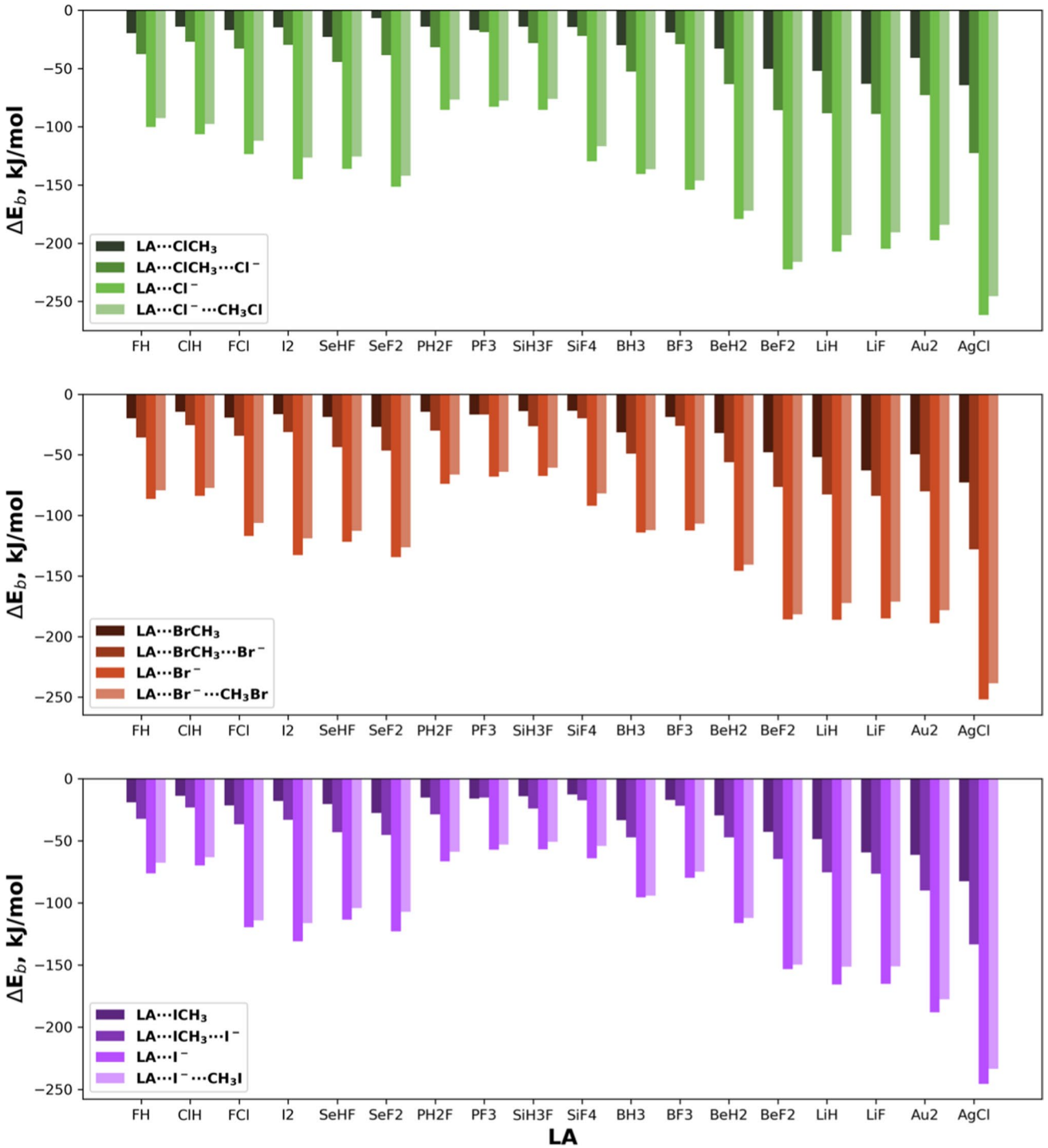

Fig. 1 BSSE corrected electronic binding energies, ΔE_b (kJ·mol^{-1}), for the interactions LA···XCH_3, LA ···X^- and between the LA and the binary complexes in the reactants (LA···X^-···CH_3X) and products (LA···XCH_3···X^-) with X = Cl, Br and I at the M06-2X/6–311++G(d,p)/def2-TZVPD computational level

interaction along the reaction path involving the three stationary points. How will the LA affect both sides (reactants and products) of the reaction? Will the LA affect the transition barriers? It is worth noting that the reactants in this study are the molecular complexes (MC), which represent a minimum between the separated reagents (products) and the TS.

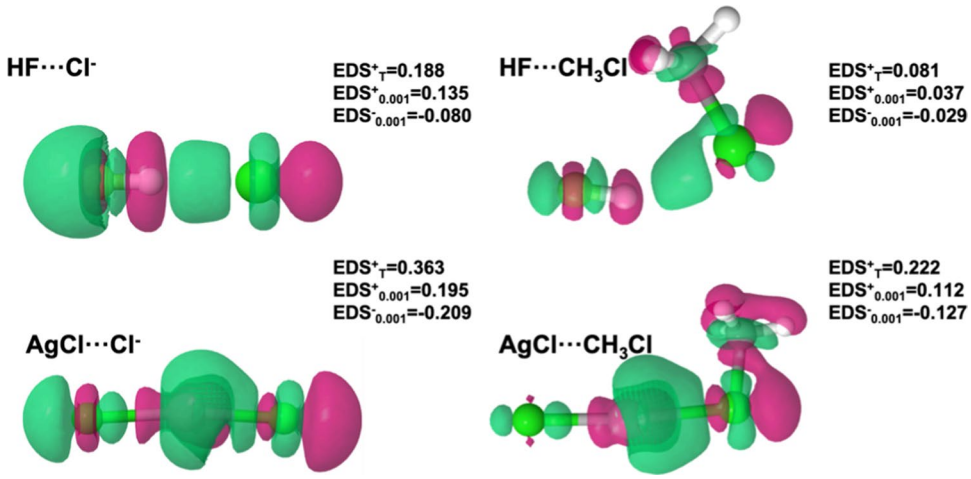

Fig. 2 Electron density shift (EDS) maps at the 0.001 a.u. cut-off for the interaction between HF/AgCl with Cl^-/CH_3Cl. Magenta and green areas correspond to regions of decrease and increase of electron density, respectively. EDS^+_T indicates the total increment of charge (in e^-) displaced, while $EDS^+_{0.001}$/$EDS^-_{0.001}$ corresponds to the increase and decrease of charge at the 0.001a.u. cut-off

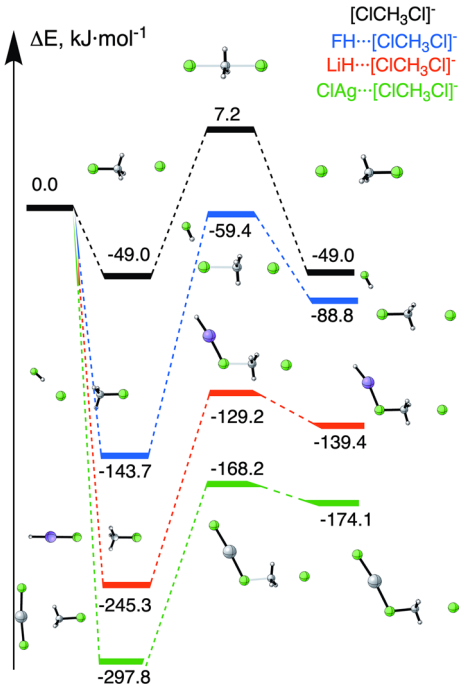

Fig. 3 Energy profile for some representative systems at the M06-2X/6–311++G(d,p)/def2-TZVPD computational level. Entrance channel is referred to the sum of the energies of the isolated monomers: $E(LA)+E(XCH_3)+E(X^-)$

The potential energy surfaces for all the cases studied are summarised in Table S3, and some representative systems for X = Cl are plotted in Fig. 3. In the investigated systems, the interaction between the LA and the anion X^- increases the stability of the reactant with reference to the parent reaction. It is important to highlight that in the presence of strong LAs, the X^- anion binds to the LA causing the resulting molecular complex to deviate from the C–X bond axis. This effect has large implications on the reactivity, since not only the LA binds strongly with the anion (Fig. 1) but also, in those cases, the LA displaces the anion out of the reaction path, *i.e.* the one aligned with the X–CH_3 molecular axis. All these features were observed for the reactions involving the three halogens, X = Cl, Br and I, atoms considered.

Regarding the different transition states (TS) obtained, the presence of the LA increases the transition barrier, computed as the energy difference between the pre-reactive (ternary) complex and the TS, in all the cases. The largest increases are found in the $ClCH_3Cl$ system, followed by Br and I derivatives. Regarding the nature of the interaction, pnictogen interactions (PH_2F) and weak hydrogen bond donors (for instance, HF) present the smallest variations, while BeF_2 shows the largest transition barrier (Fig. 4). All the energetic barrier for the systems in the LA presence are under the entrance channel.

The presence of the LA breaks the energetic degeneracy of the different reactions. Thus, even though the presence of LA increases the stability of the reaction products with respect to the parental reaction (-49 mol^{-1}), the reactions are reversible, i.e. the products are less stable than the MC. This is consistent with the interaction energies found on, one hand, between the LA and X^-, on the other hand between LA and CH_3X. The results indicate that the LA has a stronger binding affinity for the anions than for CH_3X. Consequently, based on the calculated data, the LA is expected to inhibit the reaction in principle.

3.2.2 Geometry

In order to study how does the presence of the LA affect the geometry of the stationary points along the $X^-\cdots CH_3X$ reaction path, the R1 distance will be considered as the distance between the anion X^- and the C from CH_3X, and R2 as the distance from the same carbon and the leaving X. In the reactants, the R2 distance is elongated about 0.04 Å due to the presence of the X^- anion in the MC of the $X^-\cdots$ H_3CX

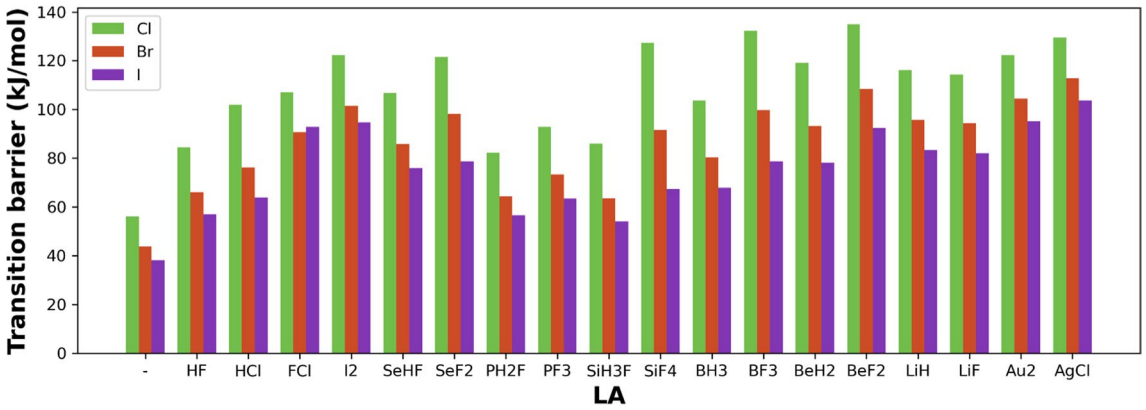

Fig. 4 Transition barriers, in kJ·mol^{-1}, calculated as the energy difference between the pre-reactive complex and the TS, for the X^-CH_3X S_N2 reactions studied at the M06-2X/6–311++G(d,p)/def2-TZVPD computational level

reaction. This elongation is reduced in the presence of the LA since the nucleophilicity of the anion is shielded, i.e. the anion has less electron density to interact with the CH_3X due to its interaction with the LA. In the same way, the X(1)–C distance increases due to the presence of LA. This increase is up to 0.96, 1.15 and 0.87 Å (Table S4) for the AgCl:$[XCH_3X]^-$ system (for X = Cl, Br and I, respectively).

Regarding the different TSs, the R1 distance is shorter than in the parental reaction while the R2 one is longer (Table S4), which indicates that the TS tends to resemble the product structure due to the presence of the LAs. In other words, it indicates that the reaction is not favoured by the presence of the LA. According to the Hammond–Leffler postulate, "the transition state resembles that of the structure closest to it in free energy" [86–88]; therefore, when the difference in X–C distances increase, the TS structures resemble the products, and consequently, the value of the TS barrier increases.

Finally, in the products the R1 distances found are longer in the presence of LA, consistent with the reduction of the electron density in the X–C bond due to the donation of X towards the LA. Also, in the product, the R2 distance is shorter than in the parental reaction, reinforcing again the idea of the decrease in the electron density on the CH_3X moiety and therefore increasing the interaction with the leaving anion X^-. These effects are more important for the stronger LAs, indicating their influence on the reaction, particularly in the electron density relocation.

A Steiner–Limbach relationship [89–92] is obtained for the C–X distances in the complexes using the "R1-R2" and "R1 + R2" parameters (Fig. 5). The "R1-R2" parameter is a measure of the asymmetry of the system. It is 0.0 in the symmetric TS of the LA free $X^-\cdots CH_3X$ reactions and increases in absolute value for the MC and products. The "R1 + R2" parameter indicates the distance between the two halogen atoms in each structure. Both parameters are useful

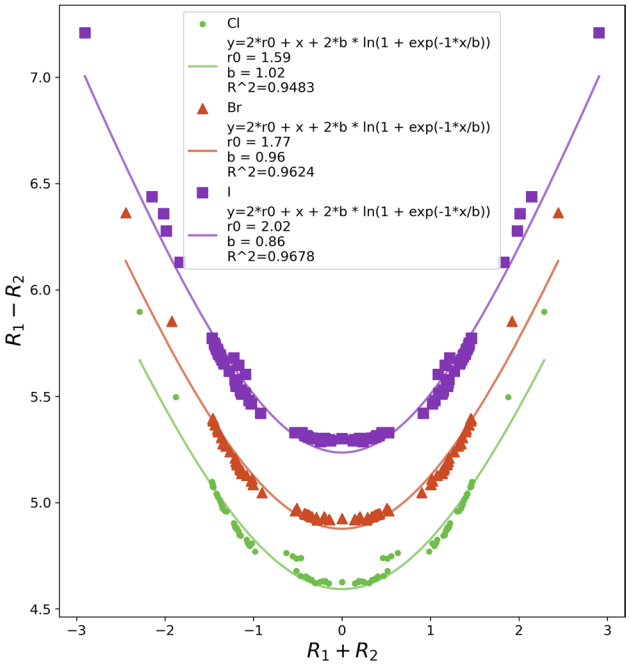

Fig. 5 Steiner–Limbach plot of the stationary points in the presence/absence of LA

to show how the presence of LA affect the geometry of MC or products, and particularly the asymmetry in the system. In principle, plotting "R1 + R2" (intramolecular X··X distance) versus "R1-R2" (asymmetry) could show that systems with longer X···X distances exhibit more asymmetry. Figure 5 clearly shows that the distance between the halogen atoms decreases as they tend towards the TS being the "R1 + R2" parameter minimum in the symmetric TS and increases in the MC and products. The strongest the interaction between LA and $[XCH_3X]^-$ system, the larger R1 + R2 and R1-R2

values. This is an indication of how the LA modifies the structure of $[XCH_3X]^-$ upon complexation.

3.2.3 IGMPlot and EDS analysis

Due to the interaction established between the different LAs and the halogen atom X(1), a redistribution of the electron density (ED) in the $[XCH_3X]^-$ donor counterpart, takes place. This involves the interaction between X(1) and LA, concomitantly with the formation of X(1)–C and dissociation of C–X(2) bonds. Therefore, in order to shed light on the mechanism from the ED perspective, an independent gradient model (IGM) analysis has been undertaken.

The IGM δg descriptor quantifies the electron density clash between two given fragment sources (atoms or molecules). Thus, it accounts for the tendency of electrons to be shared between both interacting moieties. In fact, the two-dimensional (IGM 2D) plot of δg as a function of the signed ED leads to a picture (Fig. 6) where one or more peaks (δg^{peak}) appear, leading to a characteristic signature of the interaction present in the system. δg^{peak} values can be associated to a type of interaction (on an absolute scale from non-covalent to covalent). Furthermore, the Δg integrated value assesses the interaction strength (see Computational details section for more details).

The IGM 2D-fingerprint of the interaction between two fragments: LA and $[XCH_3X]^-$ in the reactants, TS and products complexes presents δg^{peak} values found in a wide range 0.009—0.209 a.u. (Table S5, Fig. 6). As expected, these results disclose very different kinds of interactions from weak interactions to situations involving covalent features. δg^{peak} values are greater for the pre-reactive MC than for the products, owing to the negative charge on X(1) gradually decreasing along the reaction path. This is also corroborated by the Δg values (Table S5). The interactions between LA and X^- moiety (reactants) present larger integrated values than in the products ($LA\cdots XCH_3$ moiety). At the TS, the strength of the electron density clashes between the LA and

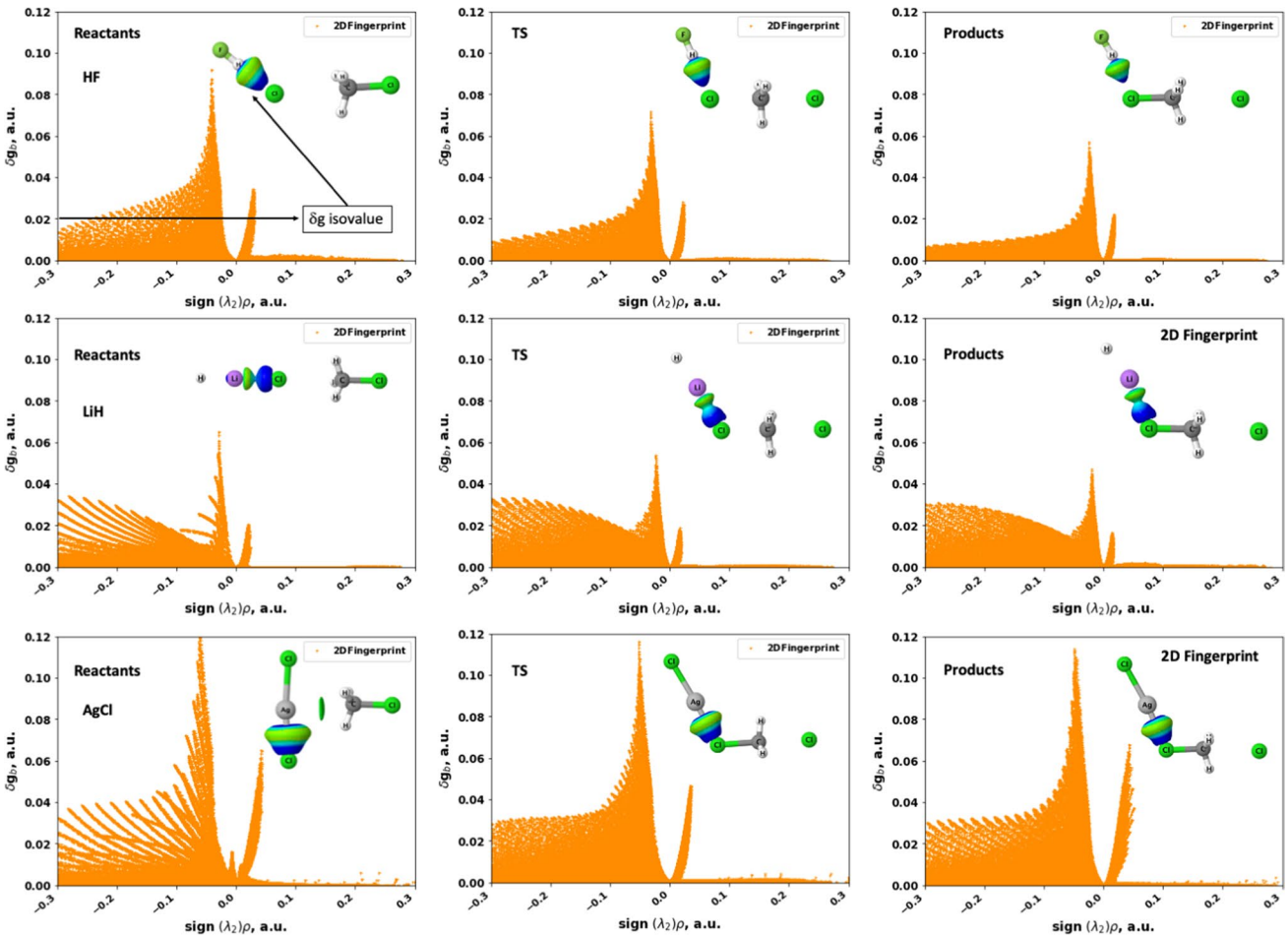

Fig. 6 IGM approach illustrated on the $BeF_2\cdots[ClCH_3Cl]^-$, $LiH\cdots[ClCH_3Cl]^-$, $HF\cdots[ClCH_3Cl]^-$ and $AgCl\cdots[ClCH_3Cl]^-$ complexes: 2D-plot signature in orange colour; 0.02 δg-isosurface associated with the interaction between LA and the reacting system; isosurfaces coloured according to the BGR scheme over the range –0.08 a.u. < sign(λ_2)ρ < 0.08 a.u

the $[XCH_3X]^-$ fragment decreases, with respect to the reactant one, since the negative charge, initially located on the $X(1)^-$ halogen, is progressively transferred to X(2). This can be seen and evaluated using electron density shift (EDS) maps [83]. However, no relationships have been found between Δg and ΔE_b value. This may be because while the Δg is focused in a single region of the space, *i.e*. on a single interaction, the ΔE_b, as a whole, accounts for several other factors (for example, electronic repulsion) for the entire system.

In Fig. 7, the electron density shifts maps have been plotted to illustrate the density displacement upon interaction with the LA. As expected from the $X^-\cdots C$ interaction, there is an increase on the electron density between both atoms due to the formation of a new bond consistent with the situation in the TS where all the electron density shift is spread along the reaction coordinate. The presence of a LA in the reactant modifies the electron density, increasing the electron density displacement in the whole complex. This is observed (Fig. 7) by the increase of the $EDS^+{}_T$ values from 0.163 e^- (no LA) to 0.301 and 0.435 e^- (HF and AgCl, respectively), which is again aligned to the binding energies and the IGM values. The same effect can be observed at the 0.001 a.u. electron density isosurface ($EDS^+{}_{0.001}$).

Finally, in order to analyse the bond formation/breaking in the reaction, the IGM–IBSI bond index has been calculated. This index does not belong to the class of conventional bond orders (Pauling, Wiberg, Mayer, …)[93–96] giving the number of electron pairs shared between two atoms, but it is rather closely related to a local bond force constant for a given atom pair. Covering a broad range of bonding cases (from non-covalent to covalent bonds), IBSI is attached to the intrinsic bond strength concept even in situations with imaginary vibrational frequency (TS) where the conventional stretching force constant is no longer connected to the restoring force concept. Therefore, IBSI is particularly suited for following bond formation and breaking in chemical reactions.

The exploration of the three stationary points along the reaction paths with a variety of LA interacting with one of the halogen atoms involved in the reaction provides a large number of IGM–IBSI values for the C–X interaction in a wide range of intermolecular distances. Those IBSI values can be used to estimate the strength of the X(1)–C and C–X(2) bonds within those stationary points. (Figure 8 shows some representative cases.) For example, the IBSI analysis shows the LA strengthening of the X(2)–C bond in the reactants while the LA weakens the same bond in the TS with respect to the reaction without the LA (Table S6) which is in agreement with associated X(2)–C elongation observed in the MC. For instance, the Cl(1)–C bond strength rises from 0.168 to 0.298 a.u. in the presence of AgCl at the TS, constituting an increase by 77% (Fig. 8).

Above all, the representation of these values (IBSI and intermolecular distances) provides excellent exponential relationships between them, as shown in Fig. 9. It is worth mentioning that while in small subsets of data (Fig S1) linear relationship is found, considering longer intermolecular distances leads to exponential relationship due to the larger data set. This relationship confirms the utility of the IBSI parameter to identify the strength of the contact which is connected in the literature with the interatomic distance.

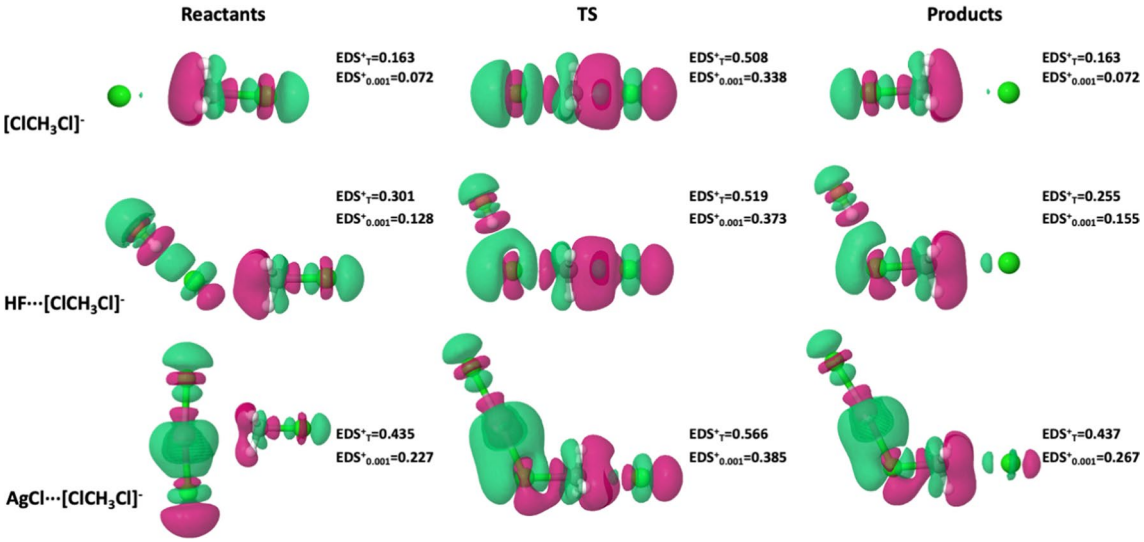

Fig. 7 Electron density shift (EDS) maps at the 0.001 a.u. cut-off. Magenta and green areas correspond to regions of decrease and increase of electron density, respectively. $EDS^+{}_T$ indicates the total increment of charge (in e^-) displaced, while $EDS^+{}_{0.001}$ corresponds to the increment of charge at the 0.001a.u. cut-off. EDS maps are obtained as: $\rho(LA[XCH_3X]^-) - \rho(LA[XCH_3]) - \rho(X^-)$

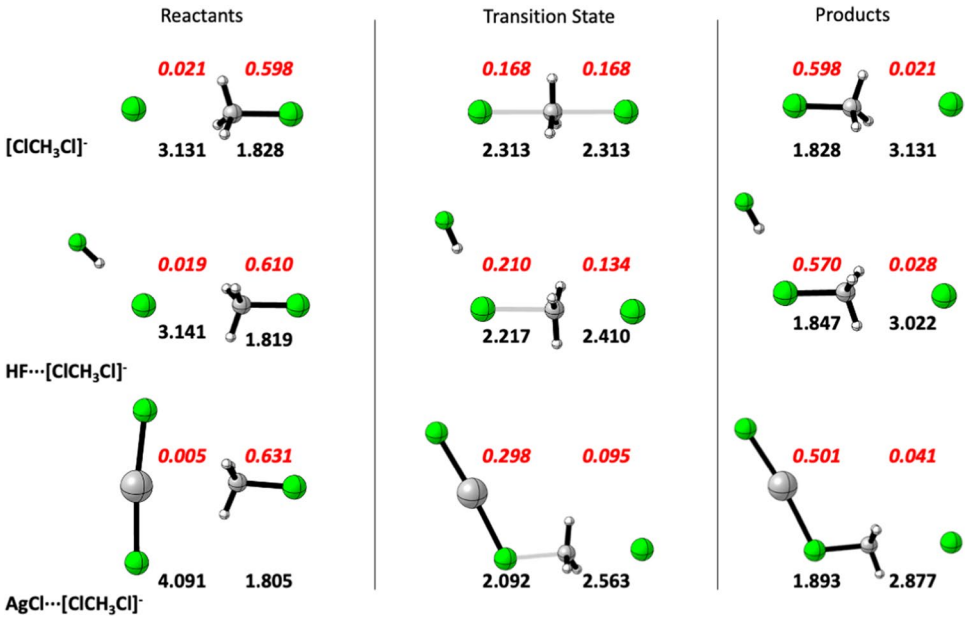

Fig. 8 Representation of the X(1)–C bond, C–X(2) distances (black, Å) and IBSI values (red italics, a.u.) in the reactants, TS and products for the $[ClCH_3Cl]^-$, $HF\cdots[ClCH_3Cl]^-$ and $AgCl\cdots[ClCH_3Cl]^-$ systems

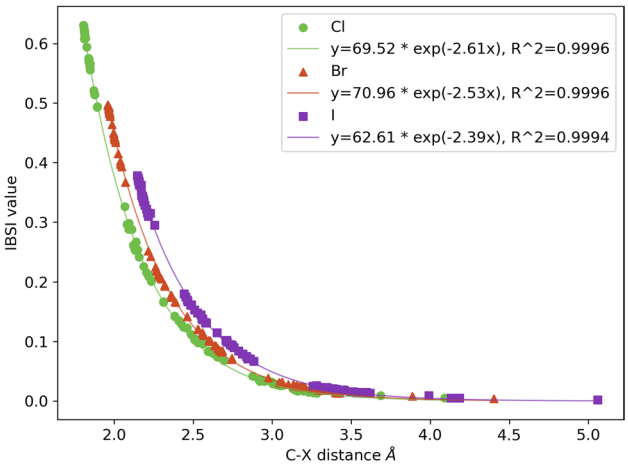

Fig. 9 IBSI values (a.u.) vs. the corresponding distance (Å) in reactants, TSs and products

4 Conclusions

The effect of the presence of LAs on a series of S_N2 reactions $[XCH_3X]^-$ (X = Cl, Br and I) has been thoroughly examined. The presence of LAs stabilise the nucleophile, MC, TS and products compared to the parental system, disrupting the energetic degeneracy of the reaction. Notably, the LA exhibits a more favourable interaction with the anionic halogen in the pre-reactive complex than with the CH_3X molecule resulting in two important energetic consequences. Firstly, the reaction is reversible since the MC are more stable than the products. Secondly, the barrier, computed as the energetic difference between the MC and the TS, increases with the presence of LAs; however, all of them are under the entrance channel in contrast with the parental one.

The nature of the interaction established between the LA and $[XCH_3X]^-$ is mainly non-covalent, though certain LAs exhibit some covalent characteristics that impact the binding energies and barriers. LA interacting through hydrogen or halogen bonds presents weak interactions with the reactants, and therefore, their influence on the pre-reaction MC, transition barriers and products is relatively mild. However, the interaction with metals, alkali, alkali earth and transition metals forming regium bonds causes larger binding energies increasing transition barriers dramatically with reference to the parent reaction. This observation is consistent across all the halogen derivatives explored.

The structural data, X(1)–C and C–X(2) features, along with the electron density analysis carried out with IGM and EDS interpreting tools, support unequivocally the energy profiles obtained and the different results obtained. Particularly, it is worth noting that IGM–IBSI values have been proved to be a good indicator of both the strength of the weak interactions, combined with the EDS and δg values, but also, they are able to quantify the bond strength in more complex situations, e.g. bond creating/breaking situations shown in the S_N2 reaction.

Supplementary Information The online version contains supplementary material available at https://doi.org/10.1007/s00214-023-03013-9.

Acknowledgements The research was financially supported by the Spanish Ministerio de Ciencia e Innovación (Project PID2021-125207NB-C32) and Science Foundation of Ireland (SFI), Grant Number 18/SIRG/5517. Thanks are given to the CTI (CSIC), the Irish Centre for High-End Computing (ICHEC), the MaSCA (Maison de la Simulation de Champagne-Ardenne, France) and the CRIANN computational centre for their continued computational support.

Author contributions II, GSS, EH and IA did the calculations. All the authors wrote parts of the manuscript text and review it when completed.

Funding Open Access funding provided by the IReL Consortium.

Declarations

Conflict of interest There are no conflicts to declare.

References

1. Hughes ED, Ingold CK (1935) 55. Mechanism of substitution at a saturated carbon atom. Part IV. A discussion of constitutional and solvent effects on the mechanism, kinetics, velocity, and orientation of substitution. J Chem Soc (Resumed). 244–55.
2. Hughes ED (1935) Hydrolysis of secondary and tertiary Alkyl Halides. J Am Chem Soc 57(4):708–709
3. Bunnet JF (1996) Physical organic terminology. After Ingold Bull Hist Chem 19:33–42
4. Olah GA (1990) Comments on IUPAC recommendations for the representation of reaction mechanisms. Acc Chem Res 23(2):31–32
5. Walden P (1896) Ueber die gegenseitige umwandlung optischer antipoden. Ber Dtsch Chem Ges 29(1):133–138
6. Walden P (1893) Ueber die vermeintliche optische activität der chlorfumarsäure und über optisch active halogenbernsteinsäure. Ber Dtsch Chem Ges 26(1):210–215
7. Hughes ED, Ingold CK, Martin RJL, Meigh DF (1950) Walden inversion and reaction mechanism: Walden inversion in unimolecular reactions of secondary and tertiary Alkyl Halides. Nature 166(4225):679–680
8. Finkelstein H (1910) Darstellung organischer jodide aus den entsprechenden bromiden und chloriden. Ber Dtsch Chem Ges 43(2):1528–1532
9. Smith MB, March J (2007) Advanced organic chemistry: reactions, mechanisms, and structure, 6th edn. Wiley-Interscience, New York
10. Bento AP, Solà M, Bickelhaupt FM (2005) Ab initio and DFT benchmark study for nucleophilic substitution at carbon (S_N2@C) and silicon (S_N2@Si). J Comput Chem 26(14):1497–1504
11. van Bochove MA, Swart M, Bickelhaupt FM (2006) Nucleophilic substitution at phosphorus (S_N2@P): disappearance and reappearance of reaction barriers. J Am Chem Soc 128(33):10738–10744
12. Pierrefixe SCAH, Fonseca Guerra C, Bickelhaupt FM (2008) Hypervalent silicon versus carbon: ball-in-a-box model. Chem Eur J 14(3):819–828
13. Hamlin TA, Swart M, Bickelhaupt FM (2018) Nucleophilic substitution (S_N2): dependence on nucleophile, leaving group, central atom, substituents, and solvent. ChemPhysChem 19(11):1315–1330
14. Hamlin TA, van Beek B, Wolters LP, Bickelhaupt FM (2018) Nucleophilic substitution in solution: activation strain analysis of weak and strong solvent effects. Chem Eur J 24(22):5927–5938
15. Vermeeren P, Hansen T, Jansen P, Swart M, Hamlin TA, Bickelhaupt FM (2020) A unified framework for understanding nucleophilicity and protophilicity in the S_N2/E2 competition. Chem Eur J 26(67):15538–15548
16. Garver JM, Fang Y-R, Eyet N, Villano SM, Bierbaum VM, Westaway KC (2010) A direct comparison of reactivity and mechanism in the gas phase and in solution. J Am Chem Soc 132(11):3808–3814
17. O'Hair RAJ, Davico GE, Hacaloglu J, Dang TT, DePuy CH, Bierbaum VM (1994) Measurements of solvent and secondary kinetic isotope effects for the gas-phase S_N2 reactions of fluoride with methyl halides. J Am Chem Soc 116(8):3609–3610
18. Vayner G, Houk KN, Jorgensen WL, Brauman JI (2004) Steric retardation of S_N2 reactions in the gas phase and solution. J Am Chem Soc 126(29):9054–9058
19. Xie J, Otto R, Mikosch J, Zhang J, Wester R, Hase WL (2014) Identification of atomic-level mechanisms for gas-phase $X^- + CH_3Y$ S_N2 reactions by combined experiments and simulations. Acc Chem Res 47(10):2960–2969
20. Leitold C, Mundy CJ, Baer MD, Schenter GK, Peters B (2020) Solvent reaction coordinate for an S_N2 reaction. J Chem Phys 153(2):024103
21. Seeley JV, Morris RA, Viggiano AA (1997) Temperature dependences of the rate constants and branching ratios for the reactions of $F^-(H_2O)0–5$ with CH_3Br. J Phys Chem A 101(25):4598–4601
22. Garver JM, Gronert S, Bierbaum VM (2011) Experimental validation of the α-effect in the gas phase. J Am Chem Soc 133(35):13894–13897
23. Yu F (2016) Dynamic reaction mechanisms of ClO^- with CH_3Cl: comparison between direct dynamics trajectory simulations and experiment. J Phys Chem A 120(11):1813–1818
24. Thomsen DL, Reece JN, Nichols CM, Hammerum S, Bierbaum VM (2014) The α-effect in gas-phase S_N2 reactions of microsolvated anions: methanol as a solvent. J Phys Chem A 118(37):8060–8066
25. Thomsen DL, Reece JN, Nichols CM, Hammerum S, Bierbaum VM (2013) Investigating the α-effect in gas-phase S_N2 reactions of microsolvated anions. J Am Chem Soc 135(41):15508–15514
26. Ren Y, Wei X-G, Ren S-J, Lau K-C, Wong N-B, Li W-K (2013) The α-effect exhibited in gas-phase S_N2@N and S_N2@C reactions. J Comput Chem 34(23):1997–2005
27. Hamlin TA, Hansen T, Vermeeren P, Bickelhaupt FM (2021) Origin of the α-effect in S_N2 reactions. Angew Chem Int Ed 60:20840–20848
28. Kubelka J, Bickelhaupt FM (2017) Activation strain analysis of S_N2 reactions at C, N, O, and F centers. J Phys Chem A 121(4):885–891
29. van Bochove MA, Swart M, Bickelhaupt FM (2009) Stepwise Walden inversion in nucleophilic substitution at phosphorus. Phys Chem Chem Phys 11(2):259–267
30. van Bochove MA, Bickelhaupt FM (2008) Nucleophilic substitution at C, Si and P: how solvation affects the shape of reaction profiles. Eur J Org Chem 2008(4):649–654
31. van Bochove MA, Swart M, Bickelhaupt FM (2007) Nucleophilic substitution at phosphorus centers (S_N2@P). ChemPhysChem 8(17):2452–2463
32. Yu F (2012) Assessment of ab initio MP2 and density functionals for characterizing the potential energy profiles of the S_N2 reactions at N center. J Comput Chem 33(15):1347–1352

33. Laerdahl JK, Uggerud E (2003) Nucleophilic identity substitution reactions. The reaction between water and protonated alcohols. Org Biomol Chem 1(16):2935–2942
34. Uggerud E (1999) Nature of the transition state in gas phase S_N2 identity reactions: correlation between nucleophilicity and proton affinity. J Chem Soc Perkin Transact 2(7):1459–1464
35. Uggerud E, Bache-Andreassen L (1999) Theoretical models and experimental data for reactions between water and protonated alcohols: substitution and elimination mechanisms. Chem Eur J 5(6):1917–1930
36. Uggerud E (2006) Nucleophilicity—periodic trends and connection to basicity. Chem Eur J 12(4):1127–1136
37. Alkorta I, Thacker JCR, Popelier PLA (2018) An interacting quantum atom study of model S_N2 reactions ($X^-\cdots CH_3X$, X = F, Cl, Br, and I). J Comput Chem 39(10):546–556
38. Gallegos González M, Costales Castro A, Martin Pendas A (2021) Energetic descriptors of steric hindrance in real space: an improved IQA picture. ChemPhysChem 22(8):775–787
39. Hu W-P, Truhlar DG (1995) Deuterium kinetic isotope effects and their temperature dependence in the gas-phase S_N2 reactions $X^- + CH_3Y$. fwdarw. $CH_3X + Y^-$ (X, Y = Cl, Br, I). J Am Chem Soc 117(43):10726–10734
40. Fernández I, Frenking G, Uggerud E (2009) The interplay between Steric and electronic effects in S_N2 reactions. Chem Eur J 15(9):2166–2175
41. Uggerud E (2009) Steric and electronic effects in S_N2 reactions. Pure Appl Chem 81(4):709
42. Ghorai MK, Tiwari DP, Jain N (2013) Lewis acid catalyzed S_N2-type ring opening of N-activated aziridines with electron-rich arenes/heteroarenes. J Org Chem 78(14):7121–7130
43. Domingo LR, Arnó M, Andrés J (1999) Influence of reactant polarity on the course of the inverse-electron-demand Diels–Alder reaction. A DFT study of regio- and stereoselectivity, presence of Lewis acid catalyst, and inclusion of solvent effects in the reaction between nitroethene and substituted ethenes. J Org Chem 64(16):5867–5875
44. Domingo LR, Ríos-Gutiérrez M, Pérez P (2020) Unveiling the Lewis acid catalyzed Diels–Alder reactions through the molecular electron density theory. Molecules [Internet]. 25(11):2535
45. Vermeeren P, Hamlin TA, Fernández I, Bickelhaupt FM (2020) How Lewis acids catalyze Diels-Alder reactions. Angew Chem Int Ed 59(15):6201–6206
46. Otto S, Bertoncin F, Engberts JBFN (1996) Lewis acid catalysis of a Diels–Alder reaction in water. J Am Chem Soc 118(33):7702–7707
47. Alkorta I, Elguero J, Frontera A (2020) Not only hydrogen bonds: other noncovalent interactions. Crystals 10(3):180
48. Scheiner S. (1997) Hydrogen bonding: a theoretical perspective. Truhlar DG, editor. New York: Oxford University Press.
49. Grabowski SJ (2021) Understanding hydrogen bonds: theoretical and experimental views. RSC, London, p 2020
50. Cavallo G, Metrangolo P, Milani R, Pilati T, Priimagi A, Resnati G et al (2016) The halogen bond. Chem Rev 116(4):2478–2601
51. Wolters LP, Schyman P, Pavan MJ, Jorgensen WL, Bickelhaupt FM, Kozuch S (2014) The many faces of halogen bonding: a review of theoretical models and methods. WIREs Comput Mol Sci 4(6):523–540
52. Turunen L, Erdélyi M (2020) Halogen bonds of halonium ions. Chem Soc Rev 49(9):2688–2700
53. Minyaev RM, Minkin VI (1998) Theoretical study of O - > X (S, Se, Te) coordination in organic compounds. Can J Chem 76(6):776–788
54. Sanz P, Yáñez M, Mó O (2003) Resonance-assisted intramolecular chalcogen-chalcogen interactions? Chem Eur J 9(18):4548–4555
55. Wang W, Ji B, Zhang Y (2009) Chalcogen bond: a sister noncovalent bond to halogen bond. J Phys Chem A 113(28):8132–8135
56. Zahn S, Frank R, Hey-Hawkins E, Kirchner B (2011) Pnicogen bonds: a new molecular linker? Chem Eur J 17(22):6034–6038
57. Scheiner S (2011) On the properties of X···N noncovalent interactions for first-, second-, and third-row X atoms. J Chem Phys 134(16):164313
58. Del Bene JE, Alkorta I, Elguero J (2015) The pnicogen bond in review: structures, binding energies, bonding properties, and spin-spin coupling constants of complexes stabilized by pnicogen bonds. In: Scheiner S (ed) Noncovalent forces. Springer International Publishing, Cham, pp 191–263
59. Bauzá A, Mooibroek TJ, Frontera A (2013) Tetrel-bonding interaction: rediscovered supramolecular force? Angew Chem Int Ed 52(47):12317–12321
60. Alkorta I, Rozas I, Elguero J (2001) Molecular complexes between silicon derivatives and electron-rich groups. J Phys Chem A 105(4):743–749
61. Grabowski SJ (2014) Tetrel bond–σ-hole bond as a preliminary stage of the S_N2 reaction. PCCP 16(5):1824–1834
62. Grabowski SJ (2015) Triel bonds, π-Hole-π-electrons interactions in complexes of boron and aluminium Trihalides and Trihydrides with acetylene and ethylene. Molecules 20(6):11297–11316
63. Grabowski SJ (2020) Triel bond and coordination of triel centres–comparison with hydrogen bond interaction. Coord Chem Rev 407:213171
64. Yáñez M, Sanz P, Mó O, Alkorta I, Elguero J (2009) Beryllium bonds, do they exist? J Chem Theory Comput 5(10):2763–2771
65. Montero-Campillo MM, Mó O, Yáñez M, Alkorta I, Elguero J. Chapter Three - The beryllium bond. In: van Eldik R, Puchta R, editors. Adv Inorg Chem. 73: Academic Press; 2019. p. 73–121.
66. Kollman PA, Liebman JF, Allen LC (1970) Lithium bond. J Am Chem Soc 92(5):1142–1150
67. Solimannejad M, Ghafari S, Esrafili MD (2013) Theoretical insight into cooperativity in lithium-bonded complexes: linear clusters of LiCN and LiNC. Chem Phys Lett 577:6–10
68. Halldin Stenlid J, Johansson AJ, Brinck T (2018) σ-Holes and σ-lumps direct the Lewis basic and acidic interactions of noble metal nanoparticles: introducing regium bonds. PCCP 20(4):2676–2692
69. Frontera A, Bauzá A (2018) Regium–π bonds: an unexplored link between noble metal nanoparticles and aromatic surfaces. Chem Eur J 24(28):7228–7234
70. Sánchez-Sanz G, Trujillo C, Alkorta I, Elguero J (2019) Understanding regium bonds and their competition with hydrogen bonds in Au2: HX complexes. ChemPhysChem 20(12):1552
71. Zhao Y, Truhlar D (2008) The M06 suite of density functionals for main group thermochemistry, thermochemical kinetics, noncovalent interactions, excited states, and transition elements: two new functionals and systematic testing of four M06-class functionals and 12 other functionals. Theor Chem Acc 120(1–3):215–241
72. Frisch MJ, Pople JA, Binkley JS (1984) Self-consistent molecular orbital methods 25. Supplementary functions for Gaussian basis sets. J Chem Phys 80(7):3265–3269
73. Weigend F, Ahlrichs R (2005) Balanced basis sets of split valence, triple zeta valence and quadruple zeta valence quality for H to Rn: design and assessment of accuracy. Phys Chem Chem Phys 7(18):3297–3305
74. Loveday O, Echeverría J (2021) Methyl groups as widespread Lewis bases in noncovalent interactions. Nat Commun 12(1):5030
75. Parthiban S, de Oliveira G, Martin JML (2001) Benchmark ab initio energy profiles for the gas-phase S_N2 Reactions $Y^- + CH_3X \rightarrow CH_3Y + X^-$ (X, Y = F, Cl, Br). Validation of hybrid DFT methods. J Phys Chem A 105(5):895–904

76. Gonzales JM, Allen WD, Schaefer HF (2005) Model identity S_N2 reactions $CH_3X + X^-$ (X = F, Cl, CN, OH, SH, NH_2, PH_2): Marcus theory analyzed. J Phys Chem A 109(46):10613–10628
77. Frisch MJ, Trucks GW, Schlegel HB, Scuseria GE, Robb MA, Cheeseman JR, et al. Gaussian 16 Rev. A.03. Wallingford, CT2016.
78. Boys SF, Bernardi F (2002) The calculation of small molecular interactions by the differences of separate total energies. Some procedures with reduced errors. Mol Phys 100(1):65–73
79. Lefebvre C, Khartabil H, Boisson J-C, Contreras-García J, Piquemal J-P, Hénon E (2018) The independent gradient model: a new approach for probing strong and weak interactions in molecules from wave function calculations. ChemPhysChem 19(6):724–735
80. Lefebvre C, Rubez G, Khartabil H, Boisson J-C, Contreras-García J, Hénon E (2017) Accurately extracting the signature of intermolecular interactions present in the NCI plot of the reduced density gradient versus electron density. PCCP 19(27):17928–17936
81. Klein J, Khartabil H, Boisson J-C, Contreras-García J, Piquemal J-P, Hénon E (2020) New way for probing bond strength. J Phys Chem A 124(9):1850–1860
82. Lefebvre C, Klein J, Khartabil H, Boisson JC, Hénon E (2023) IGMPlot: a program to identify, characterize, and quantify molecular interactions. J Comput Chem 44(20):1750–1766
83. Iribarren I, Sánchez-Sanz G, Alkorta I, Elguero J, Trujillo C (2021) Evaluation of electron density shifts in noncovalent interactions. J Phys Chem A 125(22):4741–4749
84. Hunter JD (2007) Matplotlib: a 2D graphics environment. Comput Sci Eng 9(3):90–95
85. Humphrey W, Dalke A, Schulten K (1996) VMD: visual molecular dynamics. J Mol Graph 14(1):33–38
86. Hammond GS (1955) A correlation of reaction rates. J Am Chem Soc 77(2):334–338
87. Leffler JE (1953) Parameters for the description of transition states. Science 117(3039):340–341
88. Haddon RC, Tian Z, Jiang D-E (2016) Comparative reaction diagrams for the S_N2 reaction formulated according to the leffler analysis and the hammond postulate. J Org Chem 81(9):3648–3653
89. Steiner T, Saenger W (1994) Lengthening of the covalent O–H bond in O–H…O hydrogen bonds re-examined from low-temperature neutron diffraction data of organic compounds. Acta Crystallogr Sect B 50(3):348–357
90. Steiner T (1995) Lengthening of the N-H bond in N–H…N hydrogen bonds. Preliminary structural data and implications of the bond valence concept. J Chem Soc Chem Commun 13:1331–1332
91. Ramos M, Alkorta I, Elguero J, Golubev NS, Denisov GS, Benedict H et al (1997) Theoretical study of the influence of electric fields on hydrogen-bonded acid−base complexes. J Phys Chem A 101(50):9791–9800
92. Picazo O, Alkorta I, Elguero J (2003) Large chiral recognition in hydrogen-bonded complexes and proton transfer in pyrrolo[2,3-b]pyrrole dimers as model compounds. J Org Chem 68(19):7485–7489
93. Pauling L, Brockway LO, Beach JY (1935) The dependence of interatomic distance on single bond-double bond resonance. J Am Chem Soc 57(12):2705–2709
94. Wiberg KB (1968) Application of the pople-santry-segal CNDO method to the cyclopropylcarbinyl and cyclobutyl cation and to bicyclobutane. Tetrahedron 24(3):1083–1096
95. Herndon WC (1974) Resonance theory. VI Bond orders. J Am Chem Soc 96(25):7605–7614
96. Mayer I (1986) Bond orders and valences from ab initio wave functions. Int J Quantum Chem 29(3):477–483